Eindhoven University of Technology

MASTER

Analytical and experimental LFT modeling of a double scara robot

van Helvoort, J.J.M.

Award date:
2003

Link to publication

Disclaimer
This document contains a student thesis (bachelor's or master's), as authored by a student at Eindhoven University of Technology. Student theses are made available in the TU/e repository upon obtaining the required degree. The grade received is not published on the document as presented in the repository. The required complexity or quality of research of student theses may vary by program, and the required minimum study period may vary in duration.

General rights
Copyright and moral rights for the publications made accessible in the public portal are retained by the authors and/or other copyright owners and it is a condition of accessing publications that users recognise and abide by the legal requirements associated with these rights.

- Users may download and print one copy of any publication from the public portal for the purpose of private study or research.
- You may not further distribute the material or use it for any profit-making activity or commercial gain

Analytical and experimental LFT modeling of a double scara robot

J.J.M. van Helvoort

DCT 2003.104

Master's thesis

Supervisors: Prof. dr. ir. M. Steinbuch
Dr. ir. P.F. Lambrechts
Dr. ir. M.J.G. van de Molengraft

Technische Universiteit Eindhoven
Department of Mechanical Engineering
Control Systems Technology Group

Eindhoven, November 25, 2003

Abstract

Linear Fractional Transformations (LFTs) are objects of study for robust and Linear Parameter Varying (LPV) control. For LPV control a low order LFT model is desirable. In this thesis a method for low order LFT modeling is proposed, applied to a double scara robot. From the nonlinear analytical model, derived from the equations of motion, the configuration dependent behavior of the system is derived. A structured choice for a scheduling variable is made, based on a polynomial fit of this behavior, and the order of the polynomial dependence (and hence the order of the LFT) is selected. Parameters are determined from frequency response measurements. The resulting fourth order model is validated using both frequency and time response measurements.

Summary

Linear Fractional Transformations (LFTs) are objects of study for robust and Linear Parameter Varying (LPV) control. An LFT can be regarded as a constant matrix $\begin{bmatrix} A & B \\ C & D \end{bmatrix}$ with a 'scheduling' (or 'uncertainty') block Δ placed in feedback, as is shown here graphically:

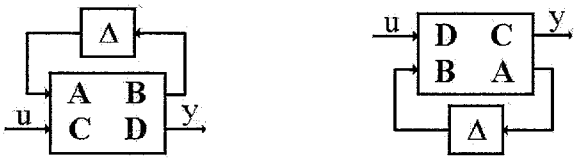

(a) Upper-LFT (b) Lower-LFT

For LPV control a low order LFT model (i.e. with a small Δ-block) is desirable. In this thesis, a systematic modeling procedure is used to construct an accurate low order LFT model of a double scara robot. This dynamical system exhibits a declining gain and shifting anti-resonance/resonance, dependent on the configuration of the system. Both phenomena affect closed loop bandwidth when using a linear controller.

A structured choice for a scheduling variable has to be made, to ensure the accuracy and low order of the model. The nonlinear analytical model of the system, starting from the equations of motion, is used to reveal the dependence of the system on the configuration. The model is Laplace transformed and it is shown that the behavior of the poles and zeros can be approximated by two second order polynomials in the chosen scheduling variable, resulting in a scheduling block with four repetitions of this variable.

From frequency response measurements, transfer functions are derived for several values of the scheduling variable. Contrary to the prediction of the analytical model, every single coefficient has to be approximated by a second order polynomial in the scheduling variable to allow more freedom in the model. Nevertheless, the resulting LFT model only contains a fourth order scheduling block (two repetitions of the scheduling variable for coefficients in numerator and two for coefficients in denominator).
The model constructed in this thesis is validated using both frequency and time domain measurements. With time response measurements, the effect of changes in the scheduling variable is investigated. It is shown that the dominant phenomena are captured by the constructed model.

Samenvatting

Lineaire Fractionele Transformaties (LFT's) zijn studie-objecten voor robuuste en Lineair Parameter Variërende (LPV) regeltechniek. Een LFT kan worden beschouwd als een constante matrix $\begin{bmatrix} A & B \\ C & D \end{bmatrix}$ met een 'plannings' (of 'onzekerheids') blok Δ in terugkoppeling hierover geplaatst, zoals hier grafisch is weergegeven:

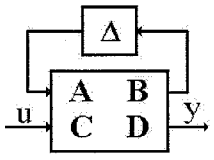

(a) boven-LFT

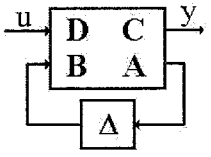

(b) onder-LFT

Voor LPV regeltechniek is een lage orde LFT model (dat wil zeggen met een klein Δ-blok) gewenst. In dit verslag wordt een systematische modelleerprocedure toegepast om een nauwkeurig lage orde LFT model op te stellen van een robot met twee knik-armen. Dit dynamische systeem laat een afnemende versterking en een verschuivende antiresonantie/resonantie zien, afhankelijk van de configuratie van het systeem. Beide fenomenen beïnvloeden de 'closed loop' bandbreedte als een lineaire regelaar wordt gebruikt.

Er moet een gestructureerde keuze voor de planningsvariabele worden gemaakt om de nauwkeurigheid en de lage orde van het model te garanderen. Het niet-lineaire analytische model van het systeem, uitgaande van de bewegingsvergelijkingen, wordt gebruikt om de afhankelijkheid van de configuratie te onthullen. Het model wordt Laplace getransformeerd en er wordt aangetoond dat het gedrag van de polen en nulpunten kan worden benaderd door twee tweede orde polynomen in de gekozen planningsvariabele, wat resulteerd in een planningsblok met vier herhalingen van deze variabele.

Uit metingen in het frequentiedomein worden overdrachtsfuncties bepaald voor verschillende waarden van de planningsvariabele. In tegenstelling tot de voorspelling uit het analytische model moet iedere coëfficient worden benaderd door een tweede orde polynoom in de planningsvariabele, om meer vrijheid toe te laten in het model. Desalniettemin heeft het resulterende LFT model slechts een vierde orde planningsblok (twee herhalingen voor de teller en twee voor de noemer).
Het model, zoals in dit verslag is opgesteld, is gevalideerd met metingen in zowel het frequentie- als het tijdsdomein. Met gemeten tijdresponsies kan

het effect van het veranderen van de planningsvariabele worden onderzocht. Er wordt aangetoond dat de dominante fenomenen worden beschreven door het opgestelde model.

Contents

Nomenclature

Latin symbols

a	perpendicular distance of lower arms to central axis
$a_{i,j}$	coefficient of normalized polynomial
$\tilde{a}_{i,j}$	coefficient of polynomial
A	mathematical expression
$b_{i,j}$	coefficient of normalized polynomial
$\tilde{b}_{i,j}$	coefficient of polynomial
d	damping constant
F_{flex}	force, exerted by spring and damper
$\mathcal{H}$	relevant part of transfer function $\frac{\Phi_2(s)}{U_2(s)}$ (i.e. third anti-resonance/resonance)
J_1	inertia of left upper arm
J_2	inertia of right upper arm
k	spring stiffness
K	total energy of system
K_m	motor constant
l_1	length of upper arms
l_2	length of lower arms
m	mass of the wrist
M	'Mass'-matrix
$p_{i,j}$	polynomial coefficient
P_i	polynomial approximation of $\tilde{P}_i$, $i = 1, 2$
$\tilde{P}_i$	exact function, defining numerator ($i = 1$) or denominator ($i = 2$)
Q	quadratic terms (in φ, ψ and their cross-product) in equations of motion
$\tilde{Q}$	quadratic terms in extended equations of motion
r	distance of wrist to central axis
T_{flex}	torque, exerted by spring and damper
u	stretch of right lower arm
u_i	control input for left motor ($i = 1$) or right motor ($i = 2$)
U_i	Laplace transform of u_i

Greek symbols

β	mathematical expression
δ	scheduling parameter
Δ	scheduling block
ξ_i	torque, exerted by motor i, $i = 1, 2$
Ξ_i	Laplace transform of ξ_i
φ	mean rotation of upper arms
φ_i	rotation of left ($i = 1$), right ($i = 2$) or fictitious ($i = 3$) upper arm
Φ_i	Laplace transform of φ_i
χ	enclosed angle of lower arms

ψ	enclosed angle of upper arms
ω_n	undamped frequency of resonance

Special symbols

$F_u(*,*)$	upper linear fractional transformation
$\mathbb{I}_{n\times n}$	identity matrix of size n
$\cot(\psi)$	cotangent of angle ψ, defined by $\cot(\psi) = \frac{\cos(\psi)}{\sin(\psi)}$

Abbreviations and acronyms

FAMM	Fast and Accurate Manipulator Module
LFT	Linear Fractional Transformation
LMI	Linear Matrix Inequality
LPV	Linear Parameter Varying
PD	Proportional Derivative
PID	Proportional Integral Derivative

1 Introduction

Last decades a lot of effort is dedicated to the development of robust and LPV (Linear Parameter Varying) control analysis and synthesis techniques for improved performance of a system with (structured) uncertainty or time-varying parameters [6, 23]. Central objects of study are Linear Fractional Transformations (LFTs). An extensive survey on the construction and manipulation of LFTs is given in [10].
In [9, 14] techniques are developed for stabilization and control of LFTs. When applying these techniques, a suitable model of the system under consideration is required, which has to be of low order to facilitate controller synthesis [17]. Often such a model is simply assumed to be available [4, 7, 14], while others only focus on parameter estimation in a given model structure, including a given scheduling variable [11, 13, 17, 8]. In none of the works however, an extensive survey of the choice of the scheduling variables as well as the order of the scheduling block is provided.

Goal of this thesis is to develop a systematic modeling procedure to construct an accurate low order LFT model for a given experimental setup. A structured choice for a scheduling variable has to be made, to ensure the accuracy and low order of the model. The nonlinear analytical model of the system, starting from the equations of motion, will be used to reveal the dependence of the system on its parameters and states and accordingly to obtain the scheduling variable and the order of dependence of the system on this scheduling variable. Experiments will be used to estimate parameter values of the LFT model as was derived from the analytical model, as well as to validate whether the low order model captures the dominant phenomena.

This thesis starts with a brief introduction to LFT modeling (section 2) and to the experimental setup as is used in this research (section 3). In section 4 an analytical model of the system is derived and the configuration dependent behavior is investigated. Parameters are determined using experiments, as is shown in section 5. The model is validated using both frequency and time response measurements (section 6).

2 Introduction to LFT modeling

In this thesis the Linear Fractional Transformation (LFT) framework is used to describe the dynamics of a double scara robot. Although this representation is widely known in literature for both robust and Linear Parameter Varying (LPV) control analysis and synthesis, a short introduction to LFT modeling is provided in this section. For more information, the reader is referred to e.g. [5, 6, 23] and references therein. In appendix A an overview is given for LFT manipulation techniques, based on the extensive survey in [10].

2.1 Notation

An LFT can be regarded as a constant matrix $\begin{bmatrix} A & B \\ C & D \end{bmatrix}$ with a 'scheduling' (or 'uncertainty') block Δ placed in feedback. In general Δ is a diagonal matrix with the Laplace operator $\frac{1}{s}$ and the uncertainties on its diagonal, see (1). $\mathbb{I}_n$ is the unity-matrix of size n, the number of repetitions of $\frac{1}{s}$ and $\mathbb{I}_{n_i}$ is the unity-matrix of size n_i, the number of repetitions of δ_i. The variable δ_i is the i^{th} scheduling or uncertainty variable.

$$\Delta = \begin{bmatrix} \frac{1}{s}\mathbb{I}_n & 0 & 0 & \dots \\ 0 & \delta_1\mathbb{I}_{n_1} & 0 & \\ 0 & 0 & \delta_2\mathbb{I}_{n_2} & \\ \vdots & & & \ddots \end{bmatrix} \tag{1}$$

The order of an LFT is defined as the total number of repetitions of the scheduling variables in the Δ-block, i.e. $\sum_{i=1,2,\dots} n_i$.
A graphical representation of an LFT is given in Fig. 1. If the Δ-block is placed over the matrix, the structure is called an upper-LFT. This structure can easily be transformed to a lower-LFT, with the Δ-block underneath the constant matrix.

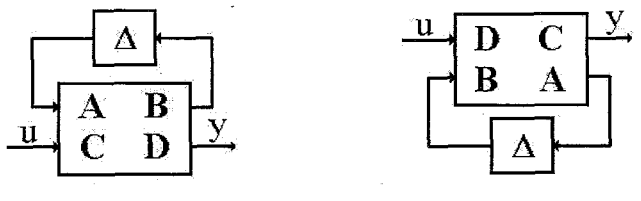

(a) Upper-LFT (b) Lower-LFT

Figure 1: *Graphical representation of LFT's*

In (2) the mathematical representation of an upper-LFT is given, with $F_u(*,*)$ the shorthand notation for the upper-LFT.

$$F_u\left(\left[\begin{array}{c|c} A & B \\ \hline C & D \end{array}\right], \Delta\right) = C\Delta\left(\mathbb{I} - A\Delta\right)^{-1} B + D \tag{2}$$

2.2 Applications

The LFT framework can be used for several modeling purposes. If the Δ-block solely consists of the Laplace operator $\frac{1}{s}$, (2) reduces to

$$F_u\left(\left[\begin{array}{c|c} A & B \\ \hline C & D \end{array}\right], \frac{1}{s}\mathbb{I}\right) = C\left(s\mathbb{I} - A\right)^{-1} B + D$$

which is the common State-Space description of a Linear Time Invariant dynamical system. When applied in robust control analysis, the uncertainty variables δ are bounded by 1 (by normalization), although the exact values are unknown. They merely represent the *possible* variation of the parameters in the model. The model is used to design controllers that are stable and meet the defined performance criteria, for all possible values of the uncertainty variables.
When applied in LPV control analysis, the scheduling variables δ are also bounded by 1. The values of δ are in general unknown *a priori* but they can be measured in real time. This extra information can be used to design an LPV controller, e.g. as in [5].

2.3 Polynomials in LFT format

When a polynomial dependence of the parameters on the scheduling variable exists, this polynomial can be converted to an LFT with the order equal to the sum of the powers of the polynomial. Note that reformulation of the polynomial may lead to a lower order LFT, as is demonstrated in appendix A.
As an example, (3) gives a quadratic polynomial in δ. This polynomial can be converted to (4), leading to a second order LFT, as given by (5):

$$\begin{aligned} P &= p_2\delta^2 + p_1\delta + p_0 && (3)\\ &= (p_2\delta + p_1)\delta + p_0 && (4)\\ &= F_u\left(\left[\begin{array}{cc|c} 0 & 1 & 0 \\ 0 & 0 & 1 \\ \hline p_2 & p_1 & p_0 \end{array}\right], \left[\begin{array}{cc} \delta & 0 \\ 0 & \delta \end{array}\right]\right) && (5) \end{aligned}$$

Note that for a given system the LFT-description is non-unique. More examples can be found in appendix A.

3 Experimental setup

The setup used for this thesis is the direct drive double scara robot, given in Fig. 2. The development of this robot was started in 1985 by Philips Center for Manufacturing Technologies (CFT) in Eindhoven as a multidisciplinary case study to design fast and accurate electromechanical servosystems.

More details about the hardware and software of the experimental setup, as is available at Eindhoven University of Technology, is given in [3, 22].

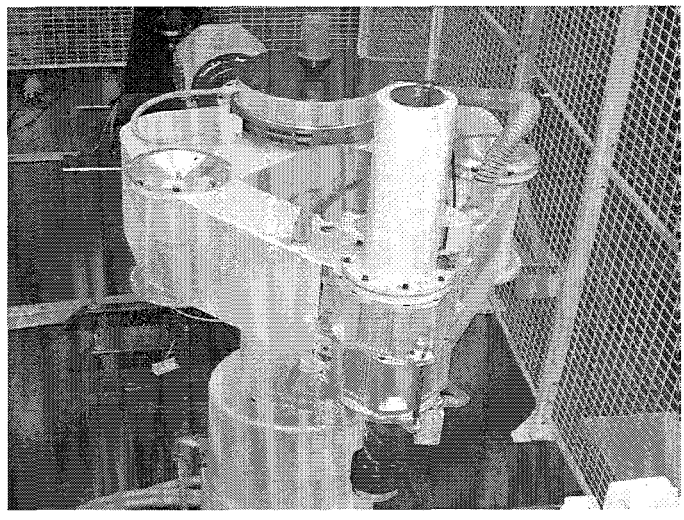

Figure 2: *Experimental setup: double scara robot at Eindhoven University of Technology*

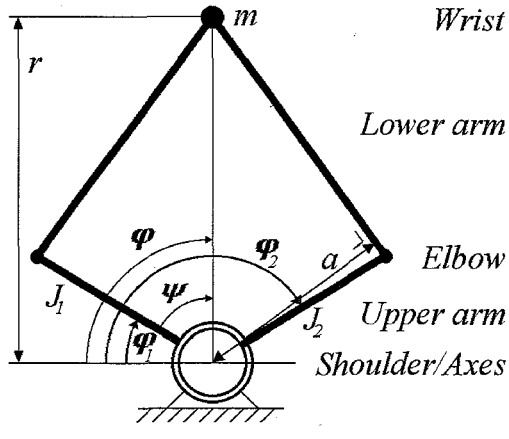

Figure 3: *Schematic top view of the experimental setup.*

The double scara robot consists of two 'upper arms' and two 'lower arms' moving in the horizontal plane, as shown in Fig. 3. The construction is like a man standing upright with his arms stretching out in front, the hands clasped together. At his hands (the 'wrist' joint), a spindle actuator is located, which will be disregarded in this thesis. However, since the wrist is the main contributor to the total mass and inertia of the system, the changing distance r of the wrist to the body and different transfer of movement of the upper arms to the movement of the wrist lead to a different inertia felt by the motors that drive the robot. These motors are situated near the 'feet' of the robot (to stick with the same metaphor), one driving the axis connected to the left upper arm, the other driving the axis connected to the right upper arm. Encoders are situated near the motors to measure angular positions [19].
Preliminary studies [16] show that due to flexibility a resonance occurs, the frequency of which changes as a function of the angle ψ. This resonance only arises in the transfer of the right motor to the right encoder, so the model in next sections will focus on this transfer.

Considering Fig. 3, angles φ_1 and φ_2 are the rotations of motor 1 (left upper arm) and motor 2 (right upper arm) respectively. Angle φ is their mean ($\varphi = \frac{\varphi_1+\varphi_2}{2}$) whereas angle ψ is the enclosed angle of the upper arms ($\psi = \frac{-\varphi_1+\varphi_2}{2}$, $\psi \in [0.5, 1.5]$ rad). Variable r is the radius at which the wrist moves around the body, as given in (6):

$$r = l_1 \cos(\psi) + \sqrt{{l_2}^2 - {l_1}^2 \sin^2(\psi)} \tag{6}$$

with l_1 the length of the upper arms and l_2 the length of the lower arms. Variable a is the perpendicular distance of the lower arms to the central axis:

$$a = \frac{l_1}{l_2} \sin(\psi) r \tag{7}$$

Parameters J_1 and J_2 represent the inertia of the upper arms and m represents the mass of the wrist.

4 Analytical modeling

In this section, an analytical model of the experimental setup is derived, to describe the shifting resonance as is encountered in preliminary studies [16]. Starting from a rigid body model, assumptions for the location of the flexibility, responsible for the configuration dependent behavior, are evaluated. The configuration dependent coefficients of the Laplace transform of the suitable solution are approximated by polynomials, both to reduce conservatism (all non-linear functions are approximated by polynomials in only one variable) and to be able to construct the corresponding LFT.

4.1 Rigid body model

First a rigid body model is considered, with only inertia of the upper arms (J_1, J_2) and a mass of the wrist (m). The mass and inertia of the lower arms are lumped into these parameters, since the wrist is the main contributor to the total inertia and mass of the system, whereas the lower arms are constructed for lightness. For definitions of parameters and variables, see previous section and in particular Fig. 3 on page 5.
The exogenous inputs are the torques on both motor axes (ξ_1, ξ_2) and the 2 degrees of freedom are their rotations (φ_1, φ_2). No potential energy is stored in the system (rigid body, no springs), so the total energy K is given by the kinetic energy (8):

$$K = \frac{1}{2}m\left(\dot{r}^2 + r^2\dot{\varphi}^2\right) + \frac{1}{2}J_1{\dot{\varphi}_1}^2 + \frac{1}{2}J_2{\dot{\varphi}_2}^2 \tag{8}$$

$$\xi_i = \frac{\partial}{\partial t}\frac{\partial K}{\partial \dot{\varphi}_i} - \frac{\partial K}{\partial \varphi_i} \qquad i = 1, 2 \tag{9}$$

With Lagrange's equation (9), expressions are derived for the rigid body motion of the system, equivalent to [15]:

$$\begin{bmatrix} \xi_1 \\ \xi_2 \end{bmatrix} = \begin{bmatrix} \frac{1}{2}mr^2 + J_1 & -\frac{1}{2}m\beta^2r^2 - J_1 \\ \frac{1}{2}mr^2 + J_2 & \frac{1}{2}m\beta^2r^2 + J_2 \end{bmatrix} \begin{bmatrix} \ddot{\varphi} \\ \ddot{\psi} \end{bmatrix} + Q(\dot{\varphi}^2, \dot{\psi}^2, \dot{\varphi}\dot{\psi}) \tag{10}$$

with

$$\beta = \frac{l_1 \sin(\psi)}{\sqrt{{l_2}^2 - {l_1}^2\sin^2(\psi)}} \tag{11}$$

$$Q = \frac{1}{2}m\beta r^2 \begin{bmatrix} \Big(\beta^2 - \beta\cot(\psi)(1+\beta^2)\Big)\dot{\psi}^2 - (\dot{\varphi}^2 + 2\dot{\varphi}\dot{\psi}) \\ \Big(-\beta^2 + \beta\cot(\psi)(1+\beta^2)\Big)\dot{\psi}^2 + (\dot{\varphi}^2 - 2\dot{\varphi}\dot{\psi}) \end{bmatrix} \tag{12}$$

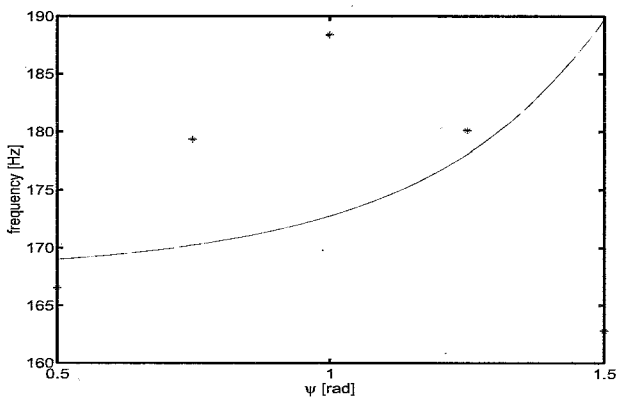

Figure 4: *Frequency of shifting resonance as a function of ψ. Model with flexibility assumed in inner axis (solid line) and measurements (stars).*

4.2 Modeling of the shifting resonance

As is already stated in [16], the mode shape belonging to the shifting resonance "is not very clear". The shifting resonance only arises in the transfer of the right motor to the right encoder, so an obvious assumption is that a flexibility is located in the central axis, for this is the element which differs the most between the left and the right arm (the axes are mounted concentric, with the left arm connected to the outer axis and the right arm connected to the inner axis). Another possible location for the flexibility is in the right lower arm, as is already suggested in [16]: "...a flexibility of some sort between the upper arm and the lower arm."

4.2.1 Flexibility in inner axis

With a flexibility in the inner axis, a configuration dependent resonance is to be expected, for the inertia of the total system changes with different ψ. A standard fourth order model can be constructed with a motor inertia (fixed) and a load inertia (configuration dependent), connected by a linear spring-damper combination.
The configuration dependency of the load inertia is derived from (10), by linearizing for zero velocity and assuming φ_1 is fixed (so $\dot{\varphi}_1 = 0$, hence $\dot{\psi} = \dot{\varphi} = \frac{\dot{\varphi}_2}{2}$). The (undamped) frequency of the resonance (ω_n) is expressed in (13), with $p \in [0, 1]$ the fraction of the inertia J_2 that is located under the flexibility, i.e. at the motor side.

$$\omega_n = \sqrt{\frac{k}{\frac{1}{4}m(\beta^2+1)r^2 + (1-p)J_2} + \frac{k}{pJ_2}} \tag{13}$$

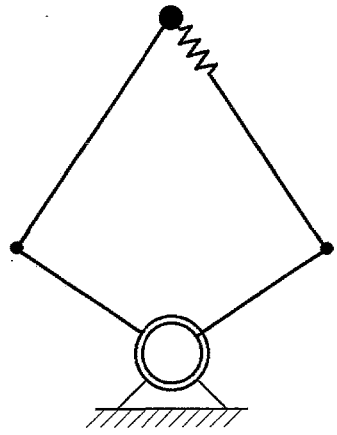

Figure 5: *Schematic topview of the robot manipulator with flexibility in the right lower arm.*

In Fig. 4 the configuration dependent behavior of the resonance frequency is depicted, for both model with flexibility in inner axis and measurements. As can be seen from the figure as well as the equation, the resonance frequency increases for increasing ψ, for every p (Proof: $\frac{\partial(\beta^2+1)r^2}{\partial\psi} < 0$ for $\psi \in [0.5, 1.5]$). This effect however does not match measurements, where the resonance frequency has a peak and declines again. Therefore the hypothesis of a flexibility in the inner axis is rejected (at least for the regarded resonance).

4.2.2 Flexibility in lower right arm

Another possible location for the flexibility in the system, responsible for the shifting resonance, is in the right lower arm. This assumption however is in contradiction with the symmetry of the robot, for the resonance is only visible in the transfer of the right motor, whereas the arms are constructed symmetrically. Although not examined in detail, this paradox may be attributed to the connection of the right lower arm to the wrist, for both arms differ slightly at this point. In Fig. 5 a schematic topview of the location of the flexibility is given.

With a flexibility in the lower arm a shifting resonance is to be expected, for when ψ changes, the angle between upper and lower arm changes and thus the ratio of the movement of the right elbow in the direction of the lower arm. This ratio is minimal when the angle between lower and upper arm is 0 or π (movement of elbow perpendicular to movement of lower arm, $\psi = 0 \vee \pi$) and maximal when the angle is $\frac{\pi}{2}$ (movement of elbow tangential to the movement of the lower arm, $\psi = \arctan\left(\frac{l2}{l1}\right) \approx 0.91$ rad).

To take into account the effect of an assumed ideal linear spring-damper combination in the right lower arm, equation (10), describing the rigid body motion, is extended with an extra DOF: φ_3. As is shown in (14) and (15), some modifications are made to the state variables.

$$\varphi = \frac{\varphi_1 + \varphi_3}{2} \tag{14}$$

$$\psi = \frac{-\varphi_1 + \varphi_3}{2} \tag{15}$$

Assumption is that φ_1 and φ_2 are still measured at the encoders, but the wrist moves as if attached to an arm with angle φ_3. This arm is connected with a spring and a damper to the right lower arm, see Fig. 6. Because the mass and inertia of the lower arm are lumped in the mass of the wrist and the inertia of the upper arm, the exact location of the spring and damper has no effect (as long as they act in the direction of the lower arm).

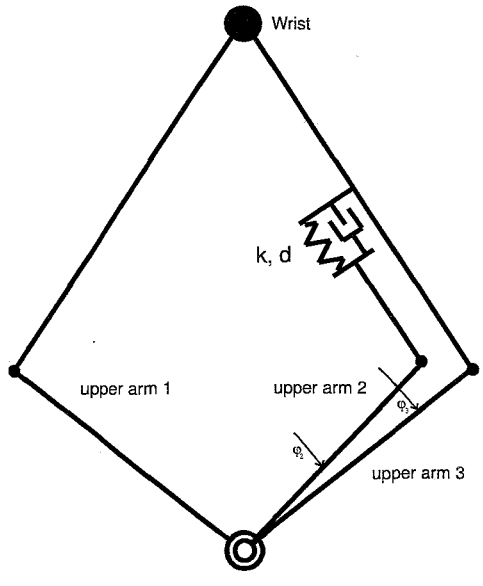

Figure 6: *Schematic representation of physical system with flexibility (topview). Upper arm 3 and φ_3 are fictitious.*

The force acting along the lower arm is a function of the relative displacement and velocity of φ_2 and φ_3. Small rotations are assumed, so upper and lower arm 2 are almost parallel to upper and lower arm 3 respectively, see Fig. 7. Angle χ is the enclosed angle of the lower arms and is defined by:

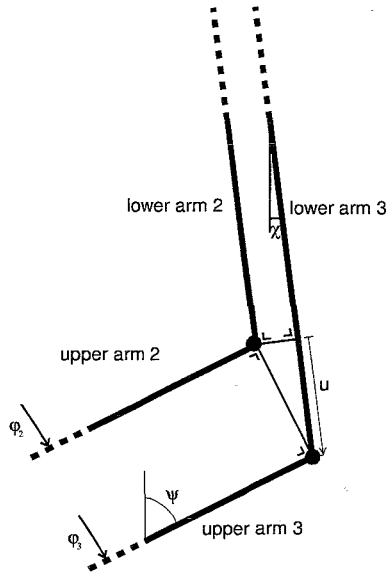

Figure 7: *Close-up of right elbow. Approximation of the stretch of the lower arm, u, with the assumption of small rotations. φ_2 is measured, whereas the wrist moves as if attached to φ_3. Lower arm 2 and 3 are longitudinally connected with a spring (not shown here).*

$$\chi = \arcsin\left(\frac{l_1}{l_2}\sin(\psi)\right) = \arctan(\beta) \tag{16}$$

With the definitions as given in (15) and (16), it can be shown that the stretch of the spring u is given by (17) and the rate $\dot{u}$ by (18) (again assuming small rotations, so ψ and consequently χ do not change). The force F_{flex} and hence the resulting torque T_{flex} are easy to derive, as is done in (19) and (20).

$$\begin{aligned}
u &= l_1 \sin(\psi+\chi)(\varphi_3-\varphi_2) \\
&= a(\varphi_3-\varphi_2) && (17)\\
\dot{u} &= a(\dot{\varphi}_3-\dot{\varphi}_2) && (18)\\
F_{flex} &= ku + d\dot{u} \\
&= a\left(k(\varphi_3-\varphi_2)+d(\dot{\varphi}_3-\dot{\varphi}_2)\right) && (19)\\
T_{flex} &= aF_{flex} = a^2\left(k(\varphi_3-\varphi_2)+d(\dot{\varphi}_3-\dot{\varphi}_2)\right) && (20)
\end{aligned}$$

The torque on motor 1, ξ_1, remains unaltered, whereas the torque on motor

2, ξ_2, is constructed of the torque from the flexibility plus the inertial torque required for the acceleration of the upper right arm. The torque on the fictitious third arm consists of the torque from the flexibility plus the torque required for the acceleration of the wrist (no external torque is applied to arm 3). The new equations are given in (21).

$$\begin{bmatrix} \xi_1 \\ \xi_2 \\ 0 \end{bmatrix} = M \begin{bmatrix} \ddot{\varphi} \\ \ddot{\psi} \\ \ddot{\varphi}_2 \end{bmatrix} + \tilde{Q}(\dot{\varphi}^2, \dot{\psi}^2, \dot{\varphi}\dot{\psi}) + \begin{bmatrix} 0 \\ -T_{flex} \\ T_{flex} \end{bmatrix} \tag{21}$$

with

$$M = \begin{bmatrix} \frac{1}{2}mr^2 + J_1 & -\frac{1}{2}m\beta^2r^2 - J_1 & 0 \\ 0 & 0 & J_2 \\ \frac{1}{2}mr^2 & \frac{1}{2}m\beta^2r^2 & 0 \end{bmatrix} \tag{22}$$

$$\tilde{Q} = \frac{1}{2}m\beta r^2 \begin{bmatrix} \Big(\beta^2 - \beta\cot(\psi)(1+\beta^2)\Big)\dot{\psi}^2 - (\dot{\varphi}^2 + 2\dot{\varphi}\dot{\psi}) \\ 0 \\ \Big(-\beta^2 + \beta\cot(\psi)(1+\beta^2)\Big)\dot{\psi}^2 + (\dot{\varphi}^2 - 2\dot{\varphi}\dot{\psi}) \end{bmatrix} \tag{23}$$

4.2.3 Laplace transform

To determine the frequency response of the system with flexibility, (21) is linearized for $\dot{\varphi} = \dot{\psi} = 0$ ($\tilde{Q}(\dot{\varphi}^2, \dot{\psi}^2, \dot{\varphi}\dot{\psi})$ drops out) and Laplace transformed. Only the relevant part, i.e. the transfer from ξ_2 to φ_2, is given.
$\Phi_2(s)$ and $\Xi_2(s)$ are the Laplace transforms of $\varphi_2(t)$ and $\xi_2(t)$ respectively.

$$s^2\Phi_2(s) = \frac{a^2}{J_2}(ds+k)(\Phi_3(s) - \Phi_2(s)) + \frac{1}{J_2}\Xi_2(s) \tag{24}$$

$$s^2\Phi_3(s) = -\frac{a^2}{A}(ds+k)(\Phi_3(s) - \Phi_2(s)) \tag{25}$$

$$\begin{aligned} \frac{\Phi_2(s)}{\Xi_2(s)} &= \frac{As^2 + a^2ds + a^2k}{J_2As^4 + (J_2+A)a^2ds^3 + (J_2+A)a^2ks^2} \\ &= \frac{\frac{1}{J_2}s^2 + \tilde{P}_1(ds+k)}{s^4 + \tilde{P}_2(ds^3 + ks^2)} \end{aligned} \tag{26}$$

with

$$\begin{aligned} A &= \frac{mr^2(m\beta^2r^2 + (\beta^2+1)J1)}{mr^2(\beta^2+1) + 4J_1} \\ \tilde{P}_1 &= \frac{a^2}{J_2A} \\ \tilde{P}_2 &= \frac{(J_2+A)a^2}{J_2A} \end{aligned}$$

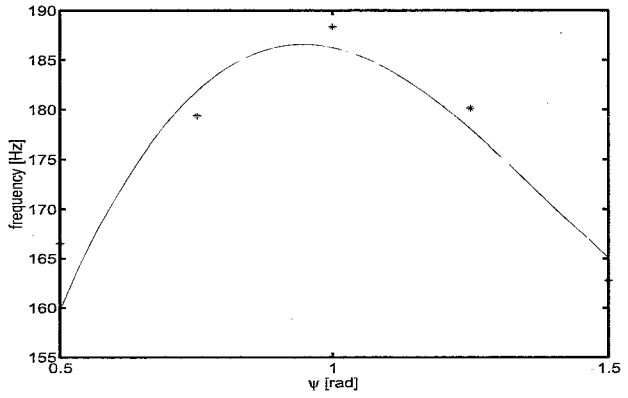

Figure 8: *Frequency of shifting resonance as a function of ψ. Model with flexibility assumed in right lower arm (solid line) and measurements (stars).*

Note that a, r and β are functions of ψ, making A, $\tilde{P}_1$ and $\tilde{P}_2$ also functions of ψ. Also note that by rewriting 26, all parameter dependence is concentrated in the functions $\tilde{P}_1$ and $\tilde{P}_2$.
In (27) and Fig. 8 the configuration dependent behavior of the frequency of the poles and zeros, derived from (26), is depicted. The bode plot of motor 2 of the system with flexibility is given in Fig. 9.

$$\omega_n = a\sqrt{\frac{(J_2 + A)k}{J_2 A}} \tag{27}$$

4.3 Transformation to LFT

To be able to describe the modeled behavior as an LFT, a polynomial fit is made of $\tilde{P}_1$ and $\tilde{P}_2$ as functions of a scheduling variable. As can be seen from (26), both for the numerator and denominator only one polynomial has to be derived (to approximate $\tilde{P}_1$ and $\tilde{P}_2$ respectively). To avoid conservatism, for both polynomials the same scheduling variable is chosen (a strong correlation exists between $\tilde{P}_1$ and $\tilde{P}_2$). Examining the exact functions to be approximated, r^2 is chosen to be the scheduling variable, for already a second order polynomial in r^2 results in a small approximation error, leading to a small but accurate scheduling block Δ. In Fig. 10 the approximations of the exact functions with both polynomials in r^2 and ψ are shown (on the left), as well as the remaining approximation error (on the right). For i = 1,2, polynomial P_i is given by:

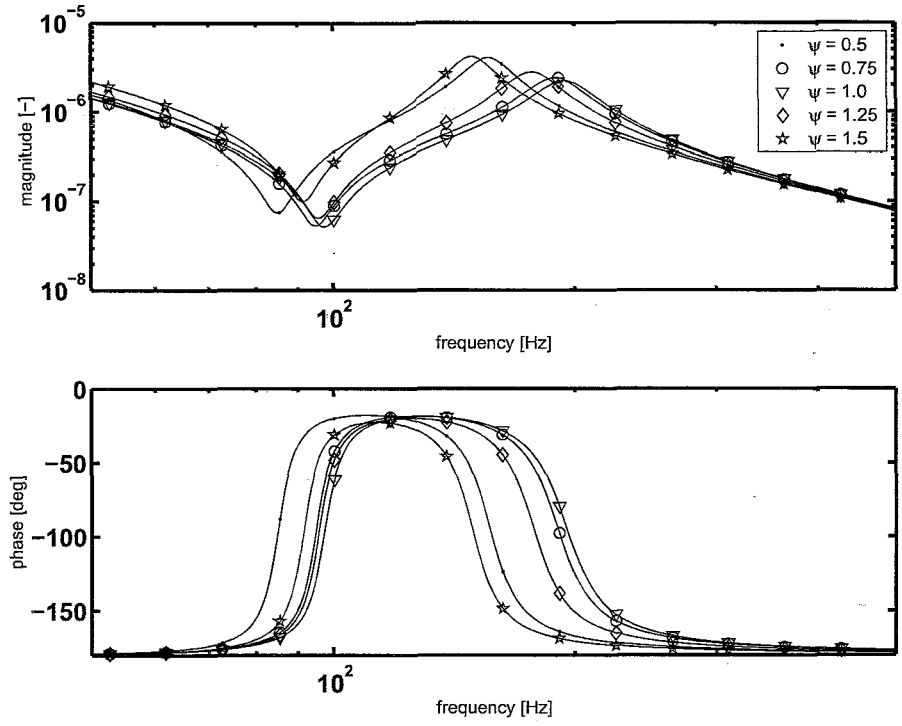

Figure 9: *Bode plot (magnitude top, phase bottom) of motor 2 to encoder 2 of system with resonance in lower arm for several values of* ψ.

$$P_i = p_{i,2}r^4 + p_{i,1}r^2 + p_{i,0} \tag{28}$$

Before converting the model with polynomials as in (28) to an LFT, r^2 is normalized, making δ the scheduling variable bounded on the interval [-1,1]:

$$r^2 = \bar{r^2} + \hat{r^2}\delta, \qquad \delta \in [-1, 1] \tag{29}$$

with

$$\begin{aligned} \bar{r^2} &= \frac{\max(r^2) + \min(r^2)}{2} \\ \hat{r^2} &= \frac{\max(r^2) - \min(r^2)}{2} \end{aligned}$$

Combining (28) and (29) yields (30). Notice that by normalizing polynomials their coefficients change whereas their structures remain unaltered.

$$P_i = c_{i,2}\delta^2 + c_{i,1}\delta + c_{i,0} \tag{30}$$

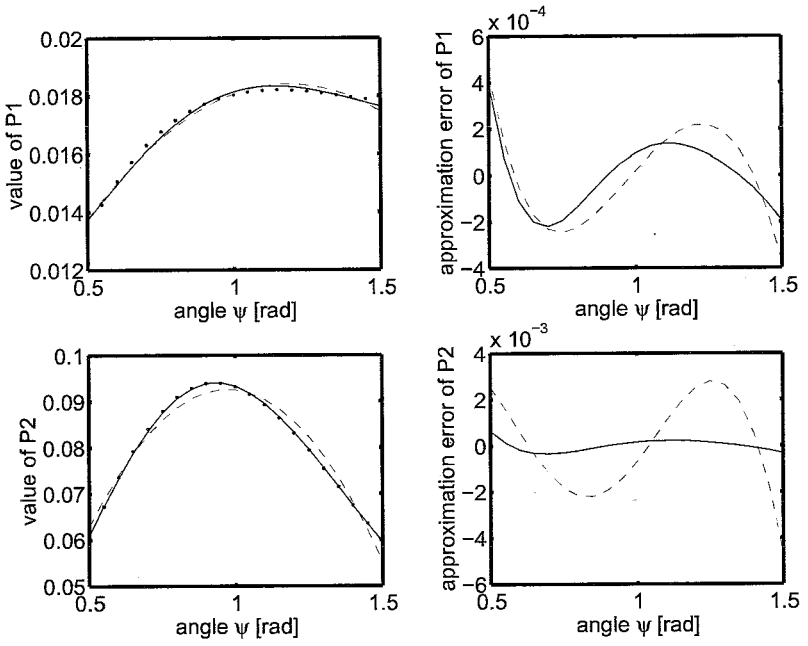

Figure 10: *Approximation of exact functions $\tilde{P}_1$ (top, left) and $\tilde{P}_2$ (bottom, left)(dots) with second order polynomials in ψ (dashed) and r^2 (solid). Observe the decreased approximation error for r^2 in comparison with ψ in the figures on the right, especially for $\tilde{P}_2$ (i.e. the denominator polynomial, defining the poles of the transfer function).*

for $i = 1, 2$, with

$$\begin{aligned} c_{i,2} &= p_{i,2}\hat{r^2}^2 \\ c_{i,1} &= 2p_{i,2}\bar{r^2}\hat{r^2} + p_{i,1}\hat{r^2} \\ c_{i,0} &= p_{i,2}\bar{r^2}^2 + p_{i,1}\bar{r^2} + p_{i,0} \end{aligned}$$

Given the definition of an upper LFT $F_u(*,*)$ as in (2), the model with polynomials P_1 and P_2 can now be converted to an LFT, as is shown below. An ideal motor is assumed with motor constant K_m (i.e. $\xi_i = K_m u_i$ with u_i the control input and $U_i(s)$ its Laplace transform).

$$\frac{\Phi_2(s)}{U_2(s)} = F_u\left(\left[\begin{array}{cc|c} A_{11} & A_{12} & B_1 \\ A_{21} & A_{22} & B_2 \\ \hline C_1 & C_2 & D \end{array}\right], \Delta\right) \tag{31}$$

with

$$
\begin{aligned}
A_{11} &= \begin{bmatrix} -dc_{2,0} & -kc_{2,0} & 0 & 0 \\ 1 & 0 & 0 & 0 \\ 0 & 1 & 0 & 0 \\ 0 & 0 & 1 & 0 \end{bmatrix} \\
A_{12} &= \begin{bmatrix} -c_{2,2} & -c_{2,1} & 0 & 0 \\ 0 & 0 & 0 & 0 \\ 0 & 0 & 0 & 0 \\ 0 & 0 & 0 & 0 \end{bmatrix} \\
A_{21} &= \begin{bmatrix} 0 & 0 & 0 & 0 \\ d & k & 0 & 0 \\ 0 & 0 & 0 & 0 \\ 0 & 0 & d & k \end{bmatrix} \\
A_{22} &= \begin{bmatrix} 0 & 1 & 0 & 0 \\ 0 & 0 & 0 & 0 \\ 0 & 0 & 0 & 1 \\ 0 & 0 & 0 & 0 \end{bmatrix} \\
B_1 &= \begin{bmatrix} K_m \\ 0 \\ 0 \\ 0 \end{bmatrix}, \qquad B_2 = \begin{bmatrix} 0 \\ 0 \\ 0 \\ 0 \end{bmatrix} \\
C_1 &= \begin{bmatrix} 0 & \frac{1}{J_2} & dc_{1,0} & kc_{1,0} \end{bmatrix} \\
C_2 &= \begin{bmatrix} 0 & 0 & c_{1,2} & c_{1,1} \end{bmatrix}, \qquad D = \begin{bmatrix} 0 \end{bmatrix} \\
\Delta &= \begin{bmatrix} \frac{1}{s}\mathbb{I}_{4\times 4} & \emptyset \\ \emptyset & \delta\mathbb{I}_{4\times 4} \end{bmatrix}
\end{aligned}
$$

5 Experiments

The motors of the experimental setup are controlled by a PC with a D-Space controller card. The movement is measured by sine-wave encoders and interpolated to 800,000 increments per revolution. A linear controller is applied ensuring a 30 to 40 Hz bandwidth of the closed loop system (variation caused by declining gain of the system).
Noise is added to the controller output and sensitivity measurements are performed, with the arm in a fixed position, to determine the transfer function of input u_2 to displacement φ_2. The measurements are repeated for several values of angle ψ (hence of r^2). The measured frequency responses are approximated by transfer functions that minimize both amplitude and phase error. As can be seen from the results depicted in Fig. 11 and 12, the overall gain as well as the frequency of the third anti-resonance/resonance changes with ψ, whereas the changes in both first and second anti-resonance/resonance are negligible.

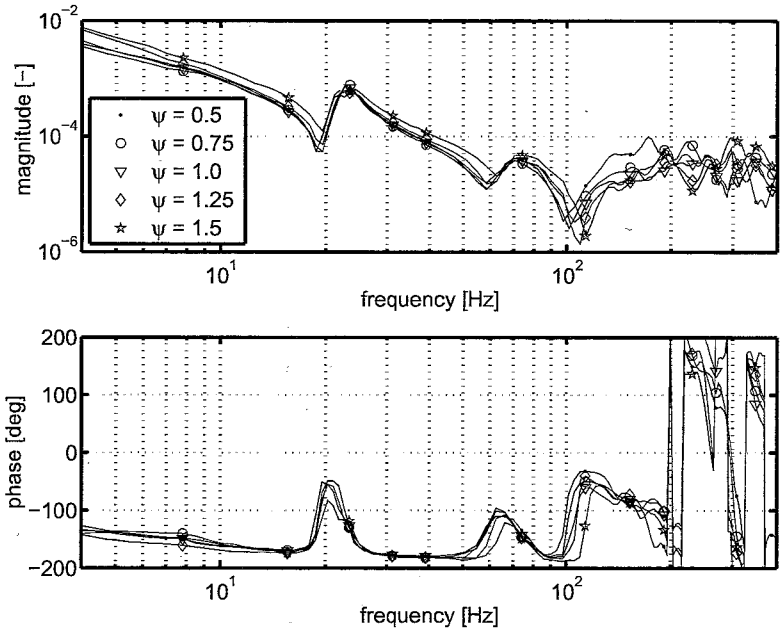

Figure 11: *Measured Frequency Responses of input u_2 to displacement φ_2 for several values of angle ψ (enclosed angle of upper arms).*

The (parameter dependent) coefficients of the fitted transfer function (32) are shown in Fig. 13 as a function of ψ. Note that only the relevant (i.e. the

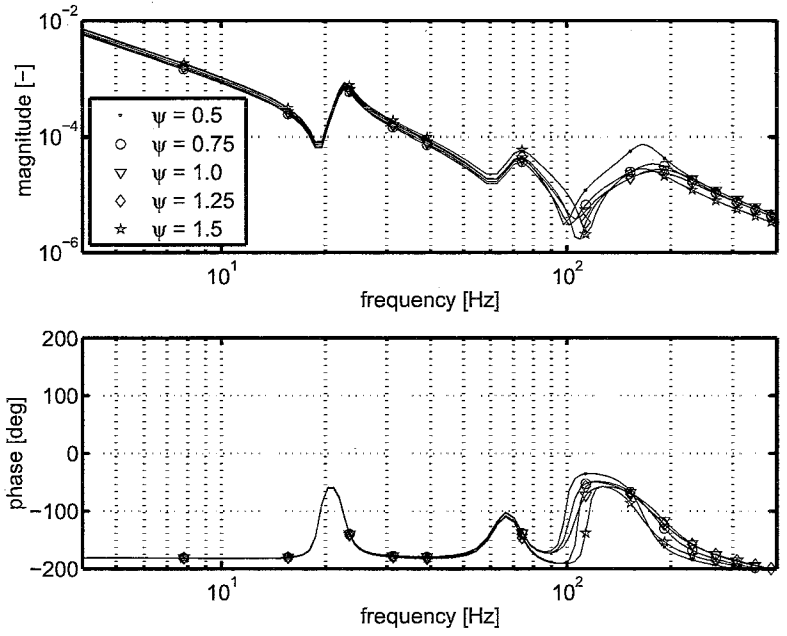

Figure 12: *Fits of measured Frequency Responses of input u_2 to displacement φ_2 for several values of angle ψ. Visible are the changing gain, fixed first and second resonances (23 and 72 Hz respectively) and shifting third resonance.*

third) anti-resonance/resonance is regarded and is denoted by $\mathcal{H}(s)$ as a part of the total transfer function $\frac{\Phi_2(s)}{U_2(s)}$.

$$\mathcal{H}(s) = \frac{a_2 s^2 + a_1 s + a_0}{s^4 + b_1 s^3 + b_0 s^2} \tag{32}$$

Whereas from the analytical model it follows that coefficient a_2 is parameter independent and coefficients a_1 and a_0 as well as coefficients b_1 and b_0 can be approximated by one polynomial, see (26), the coefficients of the fitted frequency responses show a different behavior. As can be seen from the top left of Fig. 13, a_2 changes with varying ψ, whereas in the analytical model it equals $\frac{K_m}{J_2}$. It can also be seen that the divisions $\frac{a_1}{a_0}$ as well as $\frac{b_1}{b_0}$ are not constant, and moreover, they are not equal, whereas from the analytical model it follows that $\frac{a_1}{a_0} = \frac{b_1}{b_0} = \frac{d}{k}$.
Presumably, the differences can be attributed to the lumped inertia and mass of the lower arm and the neglected friction in the robot. To model this behavior, all coefficients are independently approximated, but still by a second order polynomial in the scheduling variable r^2, as was derived from

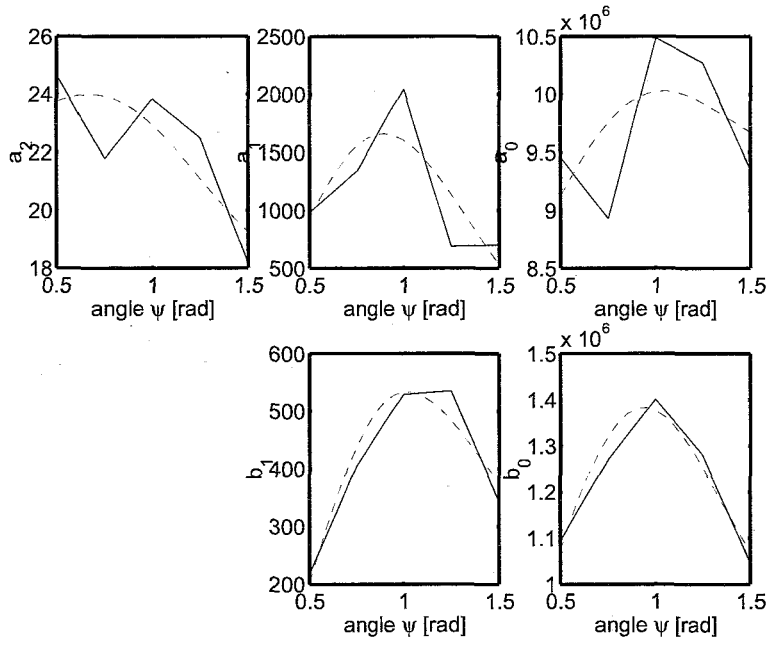

Figure 13: *Values of coefficients of the experimental transfer function (numerator top, denominator bottom) (solid line) and second order fits in* r^2 *(dashed line) as a function of* ψ.

the analytical model:

$$a_i = \begin{bmatrix} \tilde{a}_{i,2} \\ \tilde{a}_{i,1} \\ \tilde{a}_{i,0} \end{bmatrix}^T \begin{bmatrix} r^4 \\ r^2 \\ 1 \end{bmatrix} = \begin{bmatrix} a_{i,2} \\ a_{i,1} \\ a_{i,0} \end{bmatrix}^T \begin{bmatrix} \delta^2 \\ \delta \\ 1 \end{bmatrix} \qquad i = 0,1,2 \qquad (33)$$

$$b_j = \begin{bmatrix} \tilde{b}_{j,2} \\ \tilde{b}_{j,1} \\ \tilde{b}_{j,0} \end{bmatrix}^T \begin{bmatrix} r^4 \\ r^2 \\ 1 \end{bmatrix} = \begin{bmatrix} b_{j,2} \\ b_{j,1} \\ b_{j,0} \end{bmatrix}^T \begin{bmatrix} \delta^2 \\ \delta \\ 1 \end{bmatrix} \qquad j = 0,1 \qquad (34)$$

With Horner factorization it can be shown that the order of the scheduling block Δ will not increase as a consequence (only more coefficients have to be estimated). The resulting LFT is given in (35). Normalizing ($\delta \in [-1,1]$) and construction of the LFT is accomplished similar to the previous section.

$$\mathcal{H}(s) = F_u\left(\left[\begin{array}{cc|c} A_{11} & A_{12} & B_1 \\ A_{21} & A_{22} & B_2 \\ \hline C_1 & C_2 & D \end{array}\right], \Delta\right) \qquad (35)$$

with

$$
\begin{aligned}
A_{11} &= \begin{bmatrix} -b_{1,0} & -b_{0,0} & 0 & 0 \\ 1 & 0 & 0 & 0 \\ 0 & 1 & 0 & 0 \\ 0 & 0 & 1 & 0 \end{bmatrix} \\
A_{12} &= \begin{bmatrix} -1 & 0 & 0 & 0 \\ 0 & 0 & 0 & 0 \\ 0 & 0 & 0 & 0 \\ 0 & 0 & 0 & 0 \end{bmatrix} \\
A_{21} &= \begin{bmatrix} b_{1,1} & b_{0,1} & 0 & 0 \\ b_{1,2} & b_{0,2} & 0 & 0 \\ 0 & a_{2,1} & a_{1,1} & a_{0,1} \\ 0 & a_{2,2} & a_{1,2} & a_{0,2} \end{bmatrix} \\
A_{22} &= \begin{bmatrix} 0 & 1 & 0 & 0 \\ 0 & 0 & 0 & 0 \\ 0 & 0 & 0 & 1 \\ 0 & 0 & 0 & 0 \end{bmatrix} \\
B_1 &= \begin{bmatrix} 1 \\ 0 \\ 0 \\ 0 \end{bmatrix}, \qquad B_2 = \begin{bmatrix} 0 \\ 0 \\ 0 \\ 0 \end{bmatrix} \\
C_1 &= \begin{bmatrix} 0 & a_{2,0} & a_{1,0} & a_{0,0} \end{bmatrix} \\
C_2 &= \begin{bmatrix} 0 & 0 & 1 & 0 \end{bmatrix}, \qquad D = \begin{bmatrix} 0 \end{bmatrix} \\
\Delta &= \begin{bmatrix} \frac{1}{s}\mathbb{I}_{4\times 4} & \emptyset \\ \emptyset & \delta\mathbb{I}_{4\times 4} \end{bmatrix}
\end{aligned}
$$

6 Validation

In this section, results are shown of the experiments to validate the model, as is constructed in the previous sections. Both in frequency domain and in time domain, experiments will be compared to simulations.

6.1 Frequency domain validation

For frequency domain validation, the behavior of the frequency and damping of the poles and zeros is investigated. In Fig. 14 the frequency and damping of the poles and zeros of the identified model are shown as well as those of the fits of the measured frequency responses. As can be observed, the model is smoother than the measurements but they resemble one another quite closely, therefore validating the approximation of the coefficients of the transfer function and the transition to an LFT.

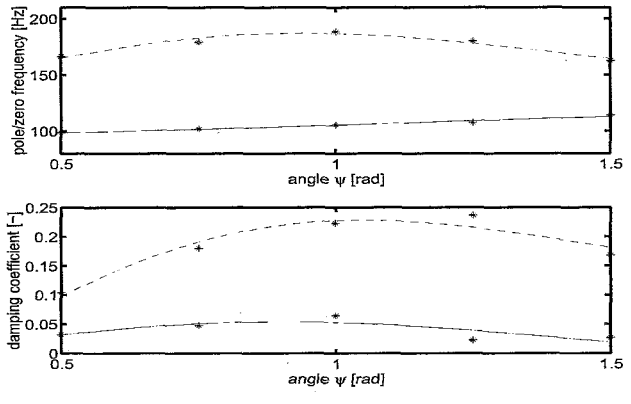

Figure 14: *Frequency (top) and damping (bottom) of the varying zeros (solid) and varying poles (dashed) in the identified model, as well as in the fits of the measured frequency responses (stars), as a function of* ψ.

6.2 Time domain validation

Time response measurements are performed to disclose the effect of a fast change in the scheduling variable, such as transient behavior. Experiments will be compared with simulations to visualize the neglected effect of a changing scheduling variable.
In the experiment, a high frequency oscillation is added to a constant velocity

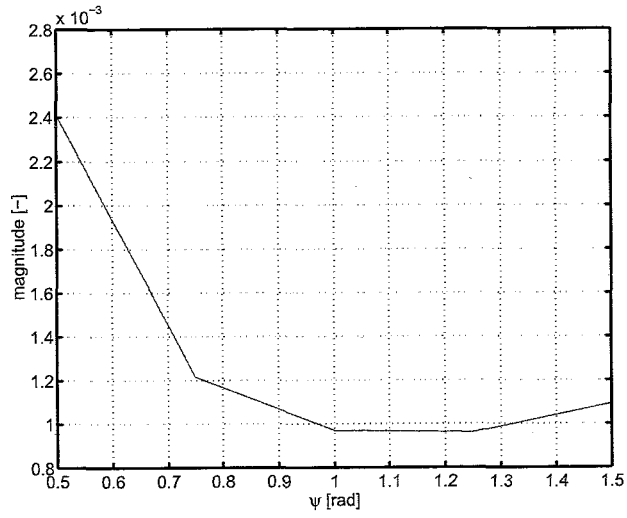

Figure 15: *Transfer function from reference to displacement of motor 2 (from fits of measured Frequency Responses)* **at 140 hz** *as a function of* ψ.

trajectory (locally around the ψ of interest) and prescribed to motor 2. The constant velocity is both in positive direction ($\dot{\psi} > 0$, arm retracting) and in negative direction ($\dot{\psi} < 0$, arm stretching). The high frequent oscillation is chosen to be a 140 hz sinusoid, because of the distinctive presence of the configuration dependent behavior at this frequency (see Fig. 15), whereas a higher frequency leads to undesirable nonlinear behavior (large noise production). To prevent saturation, the amplitude of the additive oscillation is set to 0.025 rad.

Considering the position measurement around the desired ψ (with a small symmetrical offset), the data is filtered with a bandpass filter to remove both low frequencies (i.e. the movement of the arm) and high frequencies. The filtered time response of the stroke for $\dot{\psi} < 0$ is compared to that of the stroke for $\dot{\psi} > 0$, for several values of ψ and $|\dot{\psi}|$, simulations and measurements alike.
In Fig. 16 the filtered time responses are shown for simulations with the obtained LFT model, for $\psi = 0.75$ rad and for several velocities. As can be seen, the time responses are unaffected by the speed $|\dot{\psi}|$, even for a change of direction (i.e. the solid line for $\dot{\psi} > 0$ coincides with the dashed line for $\dot{\psi} < 0$). For different values of ψ, similar results are obtained with only a change in overall gain (as might have been expected). Simulations with the non-linear equations of motion (10) yield similar results as well.

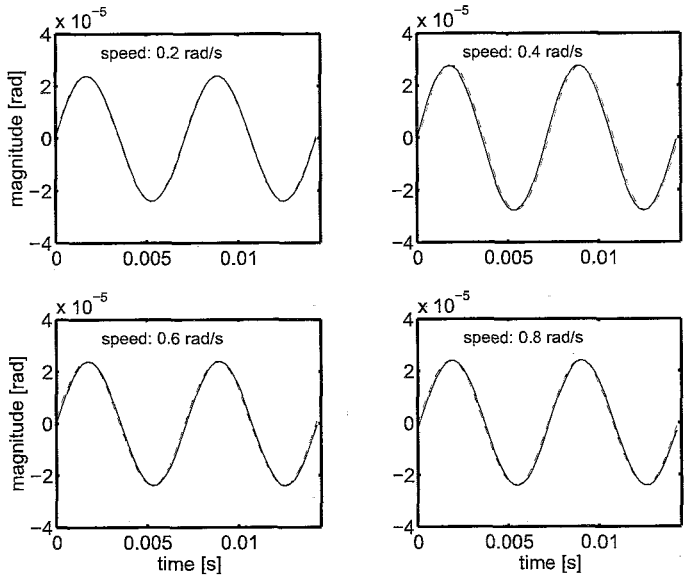

Figure 16: *Filtered time responses from simulations to an additional 140 hz oscillation of 0.025 rad on the reference around* $\psi = 0.75$ *rad and for several mean velocities* $\dot{\psi}$. *Solid line for response with* $\dot{\psi} > 0$, *dashed line for response with* $\dot{\psi} < 0$.

In Fig. 17 through 19 the filtered time responses are shown for measurements, with $\psi = 0.65$, $\psi = 0.75$ and $\psi = 0.85$ respectively and for several velocities.
If for the same velocities the three figures are compared, a decrease in gain can be observed, as was expected from Fig. 15. However, not expected from Fig. 15 is the different response for positive and negative speeds.
As can be observed from Fig. 17 through 19, a hysteresis-like effect occurs, which, once present, is nearly independent of the magnitude of the speed $|\dot{\psi}|$. It depends though on ψ, for in Fig. 19 the effect has vanished.

A possible explanation for the ψ-dependence can be found in the local rate of change as a function of ψ, see Fig. 15. At $\psi = 0.65$ and $\psi = 0.75$ a fast change of the gain can be observed, compared to $\psi = 0.85$. So a transient effect is expected to have more effect for smaller ψ.
With this explanation, however, at least some speed-dependency was expected but none was encountered.
Moreover, for $\dot{\psi} < 0$ a smaller gain was expected than for $\dot{\psi} > 0$, assuming some delay for the local transfer function. In Fig. 17 and 18, however, a larger gain can be observed for a $\dot{\psi} < 0$.

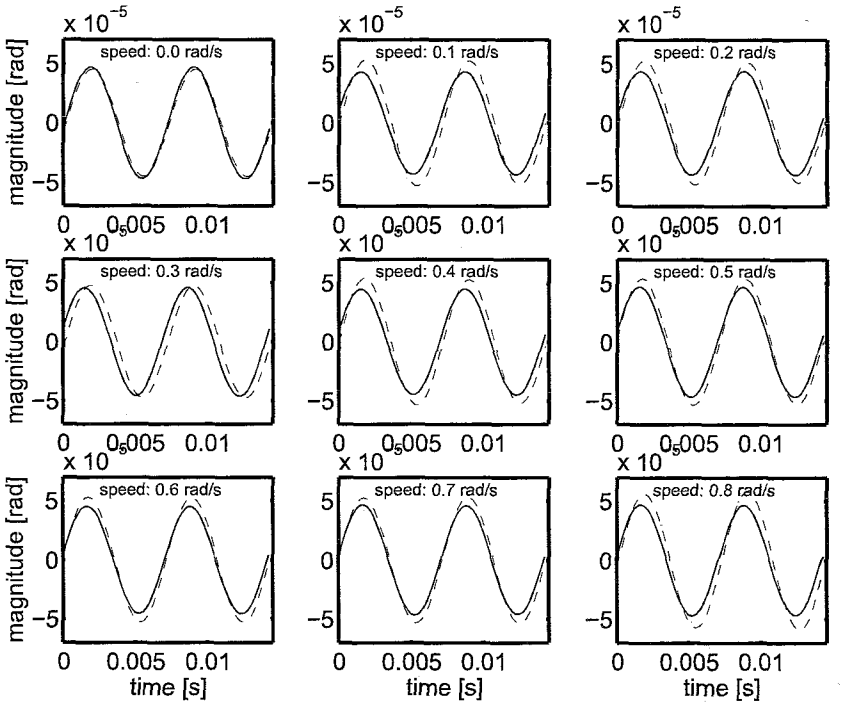

Figure 17: *Filtered time responses from measurements to an additional 140 hz oscillation of 0.025 rad on the reference around* $\psi = 0.65$ *rad and for several mean velocities* $\dot{\psi}$. *Solid line for response with* $\dot{\psi} > 0$, *dashed line for response with* $\dot{\psi} < 0$.

Despite the effect mentioned above, it can still be observed that the configuration dependency of the gain is 5 times as large as the direction dependency of the gain. So although still some unresolved phenomena occur, the model is able to describe both in frequency and in time domain the significant phenomena.

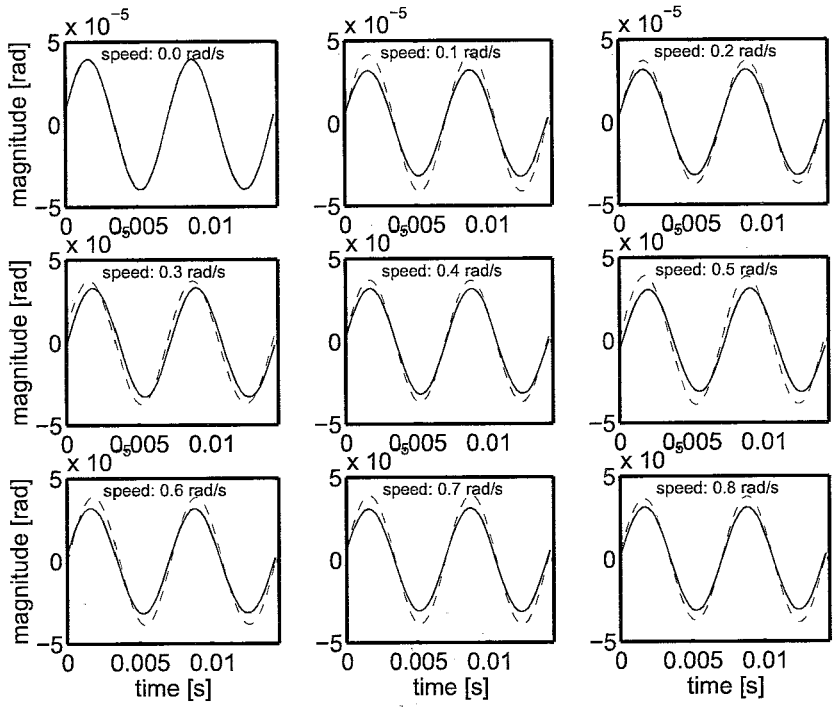

Figure 18: *Filtered time responses from measurements to an additional 140 hz oscillation of 0.025 rad on the reference around* $\psi = 0.75$ *rad and for several mean velocities* $\dot{\psi}$. *Solid line for response with* $\dot{\psi} > 0$, *dashed line for response with* $\dot{\psi} < 0$.

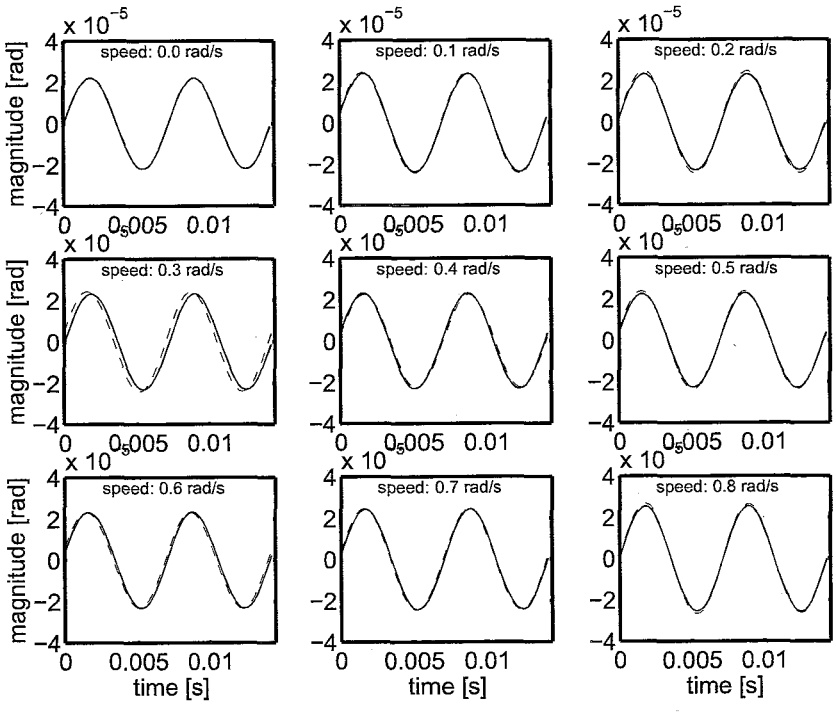

Figure 19: *Filtered time responses from measurements to an additional 140 hz oscillation of 0.025 rad on the reference around* $\psi = 0.85$ *rad and for several mean velocities* $\dot{\psi}$. *Solid line for response with* $\dot{\psi} > 0$, *dashed line for response with* $\dot{\psi} < 0$.

7 Conclusions

In this thesis, a systematic modeling procedure is applied to construct an accurate low order LFT model, using an analytical model of the system under consideration, to make a structured choice for a scheduling variable as well as the order of dependence, and experiments are used to determine the parameters of the model. This procedure is applied to a double scara robot, which exhibits a declining gain and shifting anti-resonance/resonance, dependent on the current configuration of the system. Both phenomena affect closed loop bandwidth when using a linear controller.

To analyze the dependence of the phenomena mentioned above, a nonlinear analytical model is constructed starting from the equations of motion. From the Laplace transform of this model, the configuration dependent behavior of the system is derived. A structured choice for the scheduling variable r^2 is made, based on a polynomial fit of this behavior. The order of the polynomial dependence is selected to be two, resulting in an LFT with a scheduling block with four repetitions of r^2 (two for the second order polynomial in numerator and two for the second order polynomial in denominator).

From frequency response measurements, transfer functions are derived for several values of the scheduling variable. Contrary to the prediction of the analytical model, every single coefficient has to be approximated to allow more freedom in the model. For the approximation second order polynomials in r^2 are used, as derived from the analytical model. Despite the increased freedom, the order of the resulting LFT model remains 4 (two repetitions of the scheduling variable for coefficients in numerator and two for coefficients in denominator), as can be shown by Horner factorization.

The model constructed in this thesis is validated using both frequency and time domain measurements. With time response measurements, the effect of changes in the scheduling variable is investigated. It is shown that the dominant phenomena are captured by the constructed model.

8 Recommendations

The recommendations can be divided in two main parts, i.e. model improvement and model application. They will be discussed here briefly.

In this thesis, the mass and inertia of the lower arms is lumped to the mass of the wrist and the inertia of the upper arms. Also friction is neglected. By including these phenomena in the model, the model can be improved. The equations of motion have to be extended with the factors, describing the kinetic energy of the lower arms and the nonconservative forces of the friction.

A measure for the modeling error could be investigated. A time response error for a specific trajectory could be established by looking at the difference between simulation and experiment and the model could be optimized to minimize this error. In this thesis however, the model is constructed in frequency domain, resulting in a trajectory independent model.
If first a high order model is made which is approximated by a lower order model, a truncation error is made which is bounded from above, as is shown in [10]. However since a low order model was a starting point for this thesis, no high order model is available to compare the obtained model with.

As is already mention in section 6.2, a direction dependency in time response measurements can be observed, which is not explained by the model (neither by the LFT model, nor by the nonlinear equations of motion). It is not clear what phenomenon is accountable for this effect, whether it is for instance a nonlinearity in the spring-damper or friction. This has still to be investigated. Once clear, the model could be extended to capture this phenomenon.

The next step is to construct controllers using this model. A robust controller could be designed, however the extra information of the measurable scheduling variable is not applied in this controller but merely its possible bounds. But still it would be a controller that is suitable for the entire operating range.
Next, a Linear Parameter Varying controller could be designed to incorporate the additional knowledge of the measurable scheduling variable. It should at least be as good as the robust controller, and it has the freedom to adapt to the current value of the scheduling variable.
To decrease conservatism, the maximum rate of change of the scheduling variable can be included in the controller design.

References

[1] D'Andrea, R., Khatri, S., Kalman Decomposition of Linear Fractional Transformation Representations and Minimality, *Proceedings of the American Control Conference*, Albuquerque, New Mexico, pp. 3557-3561, June 1997

[2] Belcastro, C.M., Chang, B.-C., LFT Formulation for Multivariate Polynomial Problems, *Proceedings of the American Control Conference, Philadelphia*, Pennsylvenia, pp. 1002-1007, June 1998

[3] Boeij, J.d., *Getting the FAMM-DD operational*, DCT report no. 2002.76, Eindhoven University of Technology, Eindhoven, The Netherlands, December 2002

[4] Cockburn, J.C., Morton, B.G., Linear Fractional Representations of Uncertain Systems, *Automatica*, vol. 33, no. 7, pp. 1263-1271, 1997

[5] Dettori, M., *LMI techniques for control with application to a Compact Disc player mechanism*, PhD-thesis, Delft University of Technology, Delft, The Netherlands, April 2001

[6] Doyle, J.C., Packard, A., Zhou, K., Review of LFTs, LMIs, and μ, *Proceedings of the 30th Conference on Decision and Control*, Brighton, England, pp. 1227-1232, December 1991

[7] Lambrechts, P., Terlouw, J., Bennani, S., Steinbuch, M., Parametric uncertainty modeling using LFTs, *Proceedings of the American Control Conference 1993*, San Francisco, CA, USA, pp. 267-272, 1993

[8] Lee, L.H., Poolla, K., Identification of Linear Parameter-Varying Systems via LFTs, *Proceedings of the 35th Conference on Decision and Control*, Kobe, Japan, pp. 1545-1550, December 1996

[9] Lu, W.-M., Zhou, K., Doyle, J.C., Stabilization of Uncertain Linear Systems: An LFT Approach, *IEEE Transactions on Automatic Control*, vol. 41, no. 1, pp. 50-65, January 1996

[10] Magni, J.F., *Linear Fractional Representations with a Toolbox for Use with MATLAB*, Technical report TR 240/01 Department of Systems Control and Flight Dynamics, Onera, Toulouse, France, `http://www.onera.fr/dcsd/`, December 2001

[11] Mazzaro, M.C., Movsichoff, B.A., Sánchez Peña, R.S., Robust Identification of Linear Parameter Varying Systems, *Proceedings of the American Control Conference*, San Diego, California, pp. 2282-2284, June 1999

[12] Namerikawa, T., Matsumura, F., Fujita, M., Robust Control of a Robot Manipulator using a Linear Parameter Varying Representation, *Proceedings of the IEEE International Conference on Industrial Technology*, pp. 489-492, 1996

[13] Nemani, M., Ravikanth, R., Bamieh, B.A., Identification of Linear Parametrically Varying Systems, *Proceedings of the 34th Conference on Decision & Control*, New Orleans, Louisiana, pp. 2990-2995, December 1995

[14] Packard, A., Wu, F. Control of Linear Fractional Transformations, *Proceedings of the 32nd Conference on Decision and Control*, San Antonio, Texas, pp. 1036-1041, December 1993

[15] Pasqualini, A., *Performance improvement of the FAMMDD, The Computed Torque Feedforward*, Philips CFT report CTB595-97-5269, Eindhoven, The Netherlands, September 1997

[16] Steenbakkers, M.H.A., *Evaluation and improvement of the FAMMDD, Notch- and Gain scheduling for a fast and accurate manipulator*, Master's thesis WFW.95.153, Eindhoven University of Technology, Eindhoven, The Netherlands, October 1995

[17] Steinbuch, M., van de Molengraft, R., van der Voort, A.J., Eperimental Modelling and LPV Control of a Motion System, *Proceedings of the American Control Conference 2003*, Denver, Colorado, USA, pp. 1374-1379, June 2003

[18] Stilwell, D.J., Rugh, W.J. Stability and $\mathcal{L}_2$ Gain Properties of LPV Systems, *Proceedings of the American Control Conference 1999*, San Diego, California, USA, pp. 2262-2266, June 1999

[19] Soemers, H.M.J., *FAMM: Fast and Accurate Manipulator Modules. The design of a Fast Programmable Manipulator*, CTR.545.91.0122, Philips CFT, September 1990

[20] Sznaier, M., Mazzaro, C., Inanc, T., An LMI Approach to Control Oriented Identification of LPV Systems, *Proceedings of the American Control Conference*, Chicago, Illinois, pp. 3682-3686, June 2000

[21] Tan, W., Packard, A.K., Balas, G.J., Quasi-LPV modeling and LPV Control of a Generic Missile, *Proceedings of the American Control Conference*, Chicago, Illinois, pp. 3692-3696, June 2000

[22] Verstraeten, D.C.C., *Simulation and software development of the FAMM*, DCT report no. 2003.33, Eindhoven University of Technology, Eindhoven, The Netherlands, April 2003

[23] Zhou, K., Doyle, J.C., Glover, K., *Robust and Optimal Control*, Upper Saddle River, Prentice Hall, 1996

A LFT manipulation

For calculating and manipulating Linear Fractional Transformations (LFTs), a MATLAB toolbox is developed, see [10]. This toolbox facilitates the incorporation of LFTs in the MATLAB environment, and additionally the manual is used as a guide to working with LFT's. The main principles are discussed in section 2, in this appendix some LFT manipulations are shown. For more information, the reader is referred to [10] and references therein.
In the first section the transformation from nonlinear equations to an LFT-description is described. Consequently the decomposition prior to the transformation and the order reduction after the transformation are discussed. A little note is addressed to normalization of the parameters. This section is concluded by pointing out some techniques to estimate the parameters of an LFT model from measurement data.

A.1 "From nonlinear equation to LFT"

Starting with very basic LFTs, more complex LFTs can be built. They can be put in parallel (sum, substraction) or in series (product). Without proof these manipulations are given in (36) and (37).

$$M = \begin{bmatrix} M_{11} & M_{12} \\ M_{21} & M_{22} \end{bmatrix}; \quad N = \begin{bmatrix} N_{11} & N_{12} \\ N_{21} & N_{22} \end{bmatrix}$$

$$\begin{aligned} F_u(M,\Delta^M) + F_u(N,\Delta^N) &= F_u\Big(S(M,N), \begin{bmatrix} \Delta^M & 0 \\ 0 & \Delta^N \end{bmatrix}\Big) \\ \text{with} \quad S(M,N) &= \left[\begin{array}{cc|c} M_{11} & 0 & M_{12} \\ 0 & N_{11} & N_{12} \\ \hline M_{21} & N_{21} & M_{22}+N_{22} \end{array}\right] \end{aligned} \tag{36}$$

$$\begin{aligned} F_u(M,\Delta^M) \cdot F_u(N,\Delta^N) &= F_u\Big(P(M,N), \begin{bmatrix} \Delta^M & 0 \\ 0 & \Delta^N \end{bmatrix}\Big) \\ \text{with} \quad P(M,N) &= \left[\begin{array}{cc|c} M_{11} & M_{12}N_{21} & M_{12}N_{22} \\ 0 & N_{11} & N_{12} \\ \hline M_{21} & M_{22}N_{21} & M_{22}N_{22} \end{array}\right] \end{aligned} \tag{37}$$

Two elementary LFTs are given in (38) and (39). Note that for a given system the LFT- description is not unique. Also note the parallel to dynamical systems, by replacing δ with the Laplace operator $\frac{1}{s}$.

$$a_0 + a_1\delta = F_u\left(\begin{bmatrix} 0 & 1 \\ a_1 & a_0 \end{bmatrix}, \delta\right) = F_u\left(\begin{bmatrix} 0 & a_1 \\ 1 & a_0 \end{bmatrix}, \delta\right) \tag{38}$$

$$\frac{a_0}{a_1 + a_2\delta} = F_u\left(\begin{bmatrix} -\frac{a_2}{a_1} & \frac{a_0}{a_1} \\ -\frac{a_2}{a_1} & \frac{a_0}{a_1} \end{bmatrix}, \delta\right) \tag{39}$$

By applying these algebraic manipulations and starting with the elementary LFTs, more complex LFT can be built.

A.2 Minimality

The order of an LFT is defined as the total number of repetitions of all scheduling variables in the Δ-block, see section 2.1. When applying an LFT, in general the order is preferred to be as small as possible. An LFT is said to be minimal, if there is no other equivalent representation with a smaller Δ-block. It's very hard to prove, however, that a system is minimal, so only relative minimality will be considered. In [10], a tool is developed to compute a relative minimal LFT-description. This tool is based on similarity transformations, leading to non-controllable or non-observable states. These rows and columns can then be eliminated, without changing the input/output transfer function. See also [1].
With the approach as described in section 2.3, it is obvious that the order of the LFT is equal to the sum of the orders of the δ_i's in the nonlinear equation. Then it is clear as well, that by manipulating the equations, the size of the LFT can be influenced. An example is given in (40) through (42). Of course (41) is similar to (42) (see (40)), but the size of the constructed LFT is different.

$$\begin{bmatrix} \delta_2\delta_1 \\ \delta_1 \end{bmatrix} = \begin{bmatrix} \delta_2 \\ 1 \end{bmatrix} \delta_1 \tag{40}$$

$$\begin{bmatrix} \delta_2\delta_1 \\ \delta_1 \end{bmatrix} = F_u\left(\left[\begin{array}{ccc|c} 0 & 0 & 0 & 1 \\ 0 & 0 & 0 & 1 \\ 1 & 0 & 0 & 0 \\ \hline 0 & 0 & 1 & 0 \\ 0 & 1 & 0 & 0 \end{array}\right], \begin{bmatrix} \delta_1 & 0 & 0 \\ 0 & \delta_1 & 0 \\ 0 & 0 & \delta_2 \end{bmatrix} \right) \tag{41}$$

$$\begin{bmatrix} \delta_2 \\ 1 \end{bmatrix} \delta_1 = F_u\left(\left[\begin{array}{cc|c} 0 & 0 & 1 \\ 1 & 0 & 0 \\ \hline 0 & 1 & 0 \\ 1 & 0 & 0 \end{array}\right], \begin{bmatrix} \delta_1 & 0 \\ 0 & \delta_2 \end{bmatrix} \right) \tag{42}$$

A special remark should be placed with this example, for if the first term of (40) is specified as $\delta_1\delta_2$ instead of $\delta_2\delta_1$, the minimizing routines of the MATLAB toolbox [10] will not be able to find a minimization (see (43)). However if the δ's commute (and they will if they are scalars), both representations are the same but with the second absolute minimality will not be reached.

$$\begin{bmatrix} \delta_1\delta_2 \\ \delta_1 \end{bmatrix} = \begin{bmatrix} \delta_1 & 0 \\ 0 & \delta_1 \end{bmatrix} \begin{bmatrix} \delta_2 \\ 1 \end{bmatrix}$$

$$= F_u\left(\left[\begin{array}{ccc|c} 0 & 0 & 1 & 0 \\ 0 & 0 & 0 & 1 \\ 0 & 0 & 0 & 1 \\ \hline 1 & 0 & 0 & 0 \\ 0 & 1 & 0 & 0 \end{array}\right], \begin{bmatrix} \delta_1 & 0 & 0 \\ 0 & \delta_1 & 0 \\ 0 & 0 & \delta_2 \end{bmatrix}\right) \tag{43}$$

A.3 Order reduction

Several techniques exist to reduce the order of an LFT, as will be discussed in this section. However in general with none of the current techniques a guarantee of minimality can be given (as shown in the previous section).

A.3.1 Horner factorization

As is already stated in the previous section, the size of the LFT (before being minimized) is equal to the sum of the orders of all δ_i's. So a description is preferred, where this sum is as small as possible.
With Horner factorization, the expressions of the variables in the nonlinear equation are nested resulting in a smaller sum of the orders of all δ_i's. An example is given in (44), where in the first expression the sum of all orders is 13, whereas in the second expression this sum is reduced to 8. A second example, very relevant for this thesis, is given in (45). As is demonstrated, the order of a polynomial is equal to the highest power of that polynomial.

$$2\delta_1^3\delta_2^2\delta_3 + 3\delta_1^2\delta_2^3 + 4\delta_1\delta_3 + 5 = \delta_1(\delta_1(\delta_2^2(3\delta_2 + 2\delta_1\delta_3)) + 4\delta_3) + 5 \tag{44}$$

$$a_2\delta^2 + a_1\delta + a_0 = (a_2\delta + a_1)\delta + a_0 \tag{45}$$

Horner factorization is a simple starting point to reduce the size of an LFT.

A.3.2 Tree decomposition

Tree decomposition is a generalization of Horner factorization, concerned to find the representation with the least possible appearance of parameters (i.e. of the lowest order). Two types of transformations of the representations is considered: factorization and sum decomposition. Factorization immediately reduces the order of the representation (as with Horner factorization), whereas sum decomposition has the objective to make factorization possible. Although good results can be obtained, still no guarantee for absolute minimality can be given.
In [4, 10] a more exhaustive explanation together with examples is given.

A.3.3 Matrix method

This method, originally proposed by Belcastro [2], is based on the assumption that M_{11} is nil-potent of order r. The matrix inversion can under this

condition exactly be replaced by a finite series, as is shown in (46), leading to an LFT description without matrix inversions, see (48).

$$(\mathbb{I} - M_{11}\Delta)^{-1} = \mathbb{I} + (M_{11}\Delta) + (M_{11}\Delta)^2 + \ldots + (M_{11}\Delta)^r \quad (46)$$

$$(M_{11}\Delta)^{r+1} = 0 \quad (47)$$

$$F_u\Big(\begin{bmatrix} M_{11} & M_{12} \\ M_{21} & M_{22} \end{bmatrix}, \delta\Big) = M_{21}\Delta\Big(\mathbb{I} + (M_{11}\Delta) + (M_{11}\Delta)^2 + \ldots + (M_{11}\Delta)^r\Big)M_{12} + M_{22} \quad (48)$$

Via Singular Value Decomposition and solving linear matrix equations, a low-order LFT model can be constructed. However, as is stated in [10], this method has the drawback that matrix M_{11} has to be nil-potent and problems arise with fulfilling all rank conditions ensuring the existence of a solution. This method is therefore not incorporated in the MATLAB toolbox and only mentioned here for completeness.

A.3.4 1-D order reduction

The 1-D order reduction method tries to minimize the order of the LFT once it is constructed. It considers only one δ_i at a time, the others are "disconnected" and considered as additional inputs and outputs of the system. From state space theory it can be stated that a system is minimal if and only if (A, B) is a controllable pair and (C, A) is an observable pair. In the parameter dependent case, $A = M_{11}$, $B = M_{12}$, $C = M_{21}$ (see Fig. 1) and only the delta under consideration is in the Δ-block. The 'non-observable' and 'non-controllable' states are then removed, for the input-output behavior of the system is not influenced by these states. This process is performed for all δ_is and may even be repeated to cancel the effect of the non-commutativity. See [7] for more details.

A.3.5 n-D order reduction

In [1] a method is proposed to consider all δ_is simultaneously. By similarity transformations, the 'non-observable' and 'non-reachable'/'non-controllable' states are isolated so they can be removed without altering the input-output behavior of the system. In [10] a brief explanation of this approach is given. For most systems, the 1-D and the n-D approach give similar results, however for some simple academic examples it can be shown that the n-D approach leads to better results then the 1-D approach, because simultaneously all δ_is are considered.

A.3.6 approximation of LFT

The reduction methods as discussed above are all exact reductions, i.e. $F_u(\hat{M}, \hat{\Delta}) = F_u(M, \Delta)$, with $\hat{M}$ the reduced representations of M and $\hat{\Delta}$ the appropriate

uncertainty block. Further reduction may be achieved by approximating the LFT, i.e. $\|F_u(M,\Delta) - F_u(\hat{M},\hat{\Delta})\| \leq \varepsilon$ with ε the upperbound of the approximation error (assuming that the uncertainty is normalized, see section A.4).
In [10] one method is described, the generalized Gramian approach. The generalized Gramian are the solutions X and Y of the LMI systems as described in (49) and (50), where X and Y are matrices that commute with Δ.

$$\begin{aligned} X &\geq 0 \\ M_{11}^T X M_{11} - X + M_{21}^T M_{21} &\leq 0 \qquad (49) \\ Y &\geq 0 \\ M_{11} Y M_{11}^T - Y + M_{21} M_{21}^T &\leq 0 \qquad (50) \end{aligned}$$

The product XY can be diagonalized as $XY = T\Sigma^2 T^{-1}$ and the obtained similarity transformation T applied to $F_u(M,\Delta)$. By eliminating the columns and rows of $\hat{M}$ corresponding to the null eigenvalues of matrix Σ^2, an exact reduction is made. By eliminating the columns and rows of $\hat{M}$ corresponding to the smallest non-zero eigenvalues of Σ^2, a lower order approximation is made with a maximum error of $\varepsilon = 2\sum_{i\in I}\sigma_i$, where I are the indices of the neglected eigenvalues and σ_i the square roots of the elements of Σ^2.
The selection of X and Y can be optimized by an iterative process, to minimize ε. This is implemented in an algorithm in the Matlab toolbox of [10].

A.3.7 Interpolation

If the non-linear equations are generated from measurement data, usually they are based on an interpolation between measurement points. If a very accurate approximation of the data at these points is wanted a high order fit is needed. However, one has to consider that a high order fit may lead to a high order LFT, what is unfavorable for control purposes.
Especially if noisy measurements are considered, a smooth high order fit may not be obtained. If a lower order fit is selected, the data will not be approximated as accurate, but a lower order LFT can be constructed. One should investigate what the influence of these approximations is and whether this influence is negligible compared to e.g. measurement noise. The LFT will be decreased accordingly.

A.4 Normalization

As is stated in [10], normalization of the uncertainties must be considered as the last modeling step. This is illustrated by (51) through (53), with x_i^+ and x_i^- respectively the maximum and minimum value of x_i and $\delta_i = \frac{2x_i - (x_i^+ + x_i^-)}{x_i^+ - x_i^-}$

the normalized perturbation.

$$x_1 = \frac{x_1^+ + x_1^-}{2} + \frac{x_1^+ - x_1^-}{2}\delta_1 = \bar{x}_1 + \hat{x}_1\delta_1 \quad (51)$$

$$x_2 = \frac{x_2^+ + x_2^-}{2} + \frac{x_2^+ - x_2^-}{2}\delta_2 = \bar{x}_2 + \hat{x}_2\delta_2 \quad (52)$$

$$x_1x_2 = (\bar{x}_1 + \hat{x}_1\delta_1)(\bar{x}_2 + \hat{x}_2\delta_2) = \bar{x}_1\bar{x}_2 + \bar{x}_1\hat{x}_2\delta_2 + \hat{x}_1\delta_1\bar{x}_2 + \hat{x}_1\delta_1\hat{x}_2\delta_2 \quad (53)$$

The order of the normalized product is 4 in stead of the order 2 of the product before normalization, and the current order reduction techniques are not able to return to the initial factorization.
A system $F_u(M, \Delta)$ can be normalized by some simple transformations of the matrices in M. Therefore only the upperbound x_i^+ and the lowerbound x_i^- have to be known. After normalization all δ_is will vary between -1 and $+1$. See [10] for an implementation.

A.5 "From data to LFT"

Several techniques exist to extract a model from measurement data.
Linear Time Invariant models can be made in several operating points, as is done in [10, 17]. These models are then interpolated for the scheduling parameter, generating one LFT model for the entire operating range.
Other methods identify a set of parameters for a given LFT model structure. They try to minimize the error between measurements and prediction, for instance by a gradient-based parameter estimation or a least squares estimation [8, 11, 13] or look for a model in the predefined model-set that is consistent with the measurement [20].
Main drawback of these techniques, besides that they are mostly restricted to one varying parameter and assume full state measurement, is the fixed structure and choice of scheduling variable.

B Parameter values

Estimated parameter values

In [15] parameter values are estimated using a least squares method. These values are used as a first estimate for the simulations.

Parameter	Value	
J_1	2.12	kgm^2
J_2	1.38	kgm^2
l_1	0.325	m
l_2	0.420	m
m	32.02	kg

Values of polynomial coefficients

In section 5 an LFT model is constructed. The values of the coefficients of this model are given here.

Coefficient	Value
$\tilde{a}_{2,2}$	-5.168e1
$\tilde{a}_{2,1}$	4.000e1
$\tilde{a}_{2,0}$	1.625e1
$\tilde{a}_{1,2}$	-2.645e4
$\tilde{a}_{1,1}$	1.539e4
$\tilde{a}_{1,0}$	-5.775e2
$\tilde{a}_{0,2}$	-1.734e7
$\tilde{a}_{0,1}$	7.895e6
$\tilde{a}_{0,0}$	9.131e6
$\tilde{b}_{1,2}$	-6.857e3
$\tilde{b}_{1,1}$	3.238e3
$\tilde{b}_{1,0}$	1.514e2
$\tilde{b}_{0,2}$	-8.999e6
$\tilde{b}_{0,1}$	4.870e6
$\tilde{b}_{0,0}$	7.237e5